Materials Research Express

PAPER • **OPEN ACCESS**

Comparing metal oxide thin films as transparent p-type conductive electrodes

To cite this article: C Guillén and J Herrero 2020 *Mater. Res. Express* **7** 016411

Materials Research Express

PAPER

Comparing metal oxide thin films as transparent p-type conductive electrodes

C Guillén and J Herrero

Departamento de Energía (CIEMAT), Avda. Complutense 40, Madrid-28040, Spain

E-mail: c.guillen@ciemat.es

Keywords: thin films, electrical conductivity, optical properties

OPEN ACCESS

RECEIVED
25 October 2019

REVISED
18 November 2019

ACCEPTED FOR PUBLICATION
9 December 2019

PUBLISHED
23 December 2019

Abstract

The development of transparent and p-type conductive layers remains a challenge to achieve more efficient hole collection and to combine with the most common n-type counterparts into transparent p–n junctions. Here, several candidates based on abundant materials: Cu_2O, NiO and SnO have been prepared, characterized and comparatively evaluated. Thin-film deposition methods (evaporation and sputtering) have been used along with thermal treatments (oxidation and sulfurization) to maximize the transmittance and conductivity for each material. The highest quality is achieved by $Cu_x(S, O)$ layers prepared by sulfurization of Cu_2O at 250 °C. Besides, the NiO films obtained by reactive sputtering at room temperature have a good quality to be applied on heat-sensitive substrates.

1. Introduction

Most conducting materials are opaque to visible light, while most wide band gap materials are electrically insulating. However, a class of oxide semiconductors named as transparent conductive oxides (TCOs) constitute an exception to this rule, because they are rather good conductors of electricity and simultaneously transparent in the visible region [1]. TCO materials in thin films are widely used in a variety of optoelectronic devices ranging from flat panel displays to smart windows or photovoltaic solar cells [2, 3], and other advanced photo-sensors [4]. For these applications, transparent metal oxides with high n-type conductivity are commonly used, such as Sn-doped In_2O_3, Al-doped ZnO or Sb-doped SnO_2 [2]. However, the development of high performance p-type TCOs remains a challenge to achieve more efficient hole collection and also to combine with the common n-type TCOs into transparent p–n junctions with active functionalities [5–7].

For the best design of p-type TCOs, both experimental and theoretical data about the electronic structure of metal oxides should be taken into account [7–9]. In most metal oxides, the minimum of the conduction band (CBM) is formed by metallic s orbitals that are spatially extended. Therefore, the electrons in the metal oxides have a small effective mass and high electron conduction can be achieved by an easy doping with donor impurities, resulting in n-type TCOs. On the other hand, the maximum of the valence band (VBM) is formed by oxygen 2p orbitals, which are quite localized, giving rise to a large effective mass for holes that results in very low mobilities for these charge carriers. Furthermore, the dispersion of the valence band tends to be small, and the VBM level is so deep that p-type doping is difficult [9].

Metals with d orbitals close to the O 2p can be used to favor the formation of highly hybridized orbitals that raise the VBM level and facilitate doping by holes. In this sense, Cu_2O is a good candidate because the $3d^{10}$ configuration of Cu^+ is very close to the O $2p^6$. Besides, it is intrinsically copper-deficient due to formation of copper vacancies V_{Cu} that act as a shallow and efficient hole producer [10]. The $3d^8$ configuration of Ni^{2+} is also suitable for obtaining p-type NiO, with an easy hole dopability by cation deficiency [11]. An interesting alternative is tin monoxide, because the $4d^{10}5s^2$ configuration of Sn^{2+} allows hybridization of the cation s states with the O 2p orbitals. Since the s orbitals are more delocalized than the d orbitals, this hybridization with s orbitals can lead to a greater dispersion of the valence band and therefore lower effective mass for holes than in the case of the Cu_2O, where the hybridization is performed with d orbitals [12, 13]. The calculations made on a

large set of compounds indicate that the hybridization of cation s orbital with O 2p is more pronounced for the Sn^{2+}, followed by Pb^{2+} and finally Tl^{1+}, which has the less dispersive valence band [8].

Otherwise, it has been proposed to add an anion of the type S^{2-} or P^{3-} because these have 3p orbitals more delocalized than the O 2p and can modify the valence band so that the holes effective mass decreases [7, 8]. Since the pure metal sulfides or selenides have band-gap energies lower than the corresponding oxides, a better option is the formation of oxychalcogenides, in order to decrease the effective mass of holes and maintain high values for the energy gap that allow achieve a high transparency [14]. Although both oxygen and chalcogens (S or Se) are group VI elements, the sizes of their ions are considerably different. Hence, oxygen and chalcogens do not form a solid solution in crystals and are generally spatially separated, forming a layered structure [12].

For large-scale device applications, it is now of the utmost importance to reduce the cost of the materials and preparation processes. Hence, the research is directed towards abundant materials and with low environmental impact to reduce costs in handling and security. In addition, the substitution of conventional glasses by plastic substrates, cheaper and less fragile or heavy, can significantly lower final prices and enhance the industrial viability of the preparation processes. Especially interesting is the development of thin film materials at room temperature by continuous or monolithic processes [15]. For this purpose, both evaporation and sputtering systems were built and installed in our lab, which allow the deposition of thin films of metals and metal oxides on substrates up to $30 \times 30\ cm^2$ [16, 17].

In the present work, evaporation and sputtering processes have been developed to obtain different p-type TCO films based on abundant materials. Specifically, Cu_2O, NiO and SnO oxides have been synthesized, characterized and evaluated comparatively. The deposition processes have been adjusted to achieve optimum transmittance and conductivity for each material, but also minimizing the working temperature because this means greater economy and larger application on heat-sensitive substrates. Besides, the effect of adding S^{2-} anions has been investigated by the formation of $Cu_x(S, O)$ layers by three different ways: (a) oxidation of CuS, (b) sulfurization of Cu_2O and c) direct sulfoxidation of metallic copper.

2. Methods

Evaporation and magnetron sputtering systems were used to obtain thin films of Cu_2O, $Cu_x(S, O)$, NiO and SnO on glass substrates, as grown at room temperature or after heat treatment performed under a controlled atmosphere.

Copper layers were prepared by evaporation and annealed at different temperatures (between 200 °C and 500 °C) in a tubular quartz furnace, always with flowing N_2 ($1.5\ l\ min^{-1}$) and adding O_2 flow ($0.3\ l\ min^{-1}$) for the oxidation process or elemental S (placed next to the sample in a quartz holder) for the sulfurization. Both flowing O_2 and elemental S were introduced concurrently in the process of sulfoxidation.

Besides, nickel oxide and tin oxide layers were prepared by reactive DC magnetron sputtering from the respective metallic target. The magnetism of pure Ni target involves technical problems that were avoided by using a typical non-magnetic alloy of 92%Ni:8%V [15]. After evacuation of the sputtering chamber to a base pressure of 4×10^{-4} Pa, oxygen and argon gases were introduced by independent mass flow controllers to adjust the oxygen partial pressure $O_{pp}(\%) = 100p(O_2)/[p(O_2) + p(Ar)]$, which determines the film stoichiometry. In order to improve the crystallinity of the sputtered samples, post-deposition heat treatments were performed in air at temperatures ranging from 200 °C to 500 °C for 30 min.

The structural properties of the layers were examined by x-ray diffraction (XRD) using Cu $K_{\alpha 1}$ ($\lambda = 1.54056$ Å) radiation in a Philips X'pert instrument with Bragg-Brentano $\theta - 2\theta$ configuration. Crystalline phases were identified by comparison of the measured diffraction peaks with the Joint Committee of Powder Diffraction Standards (JCPDS) files. The mean crystallite size was estimated using the Scherrer formula based on the full width at half-maximum of the main diffraction peak. The optical properties were determined in the 300–1500 nm wavelength range with a double beam spectrophotometer Perkin-Elmer Lambda 9, which has an integrating sphere to measure the total transmittance (T_t) and reflectance (R_t). In order to eliminate the interference peaks, the transmittance is corrected for reflection losses: $T(\%) = 100T_t(\%)/[100 - R_t(\%)]$. Then, the optical absorption coefficient is determined as: $\alpha = (1/t)\ln[100/T(\%)]$, including the film thickness value (t) measured by profilometry. Here, a same thickness of about 0.1 μm has been used to compare the different samples. The band-gap energy (E_g) is calculated according to direct allowed transitions: $(\alpha E)^2 = A(E - E_g)$. The electrical conductivity, carrier concentration and mobility were determined with an ECOPIA Hall Measurement System. Before electrical measurements, the samples were cut into square pieces of $1 \times 1\ cm^2$ and placed on a sample holder with four gold-plated spring loaded pins. Conductive Ag paste is added to improve pin contact to the layer. The conductivity (σ) depends on the sheet resistance (R_S) and the film thickness as: $\sigma = 1/(R_s t)$. Electrical measurements were made one or two weeks after film deposition, and no significant changes were detected by environmental exposure in the interval.

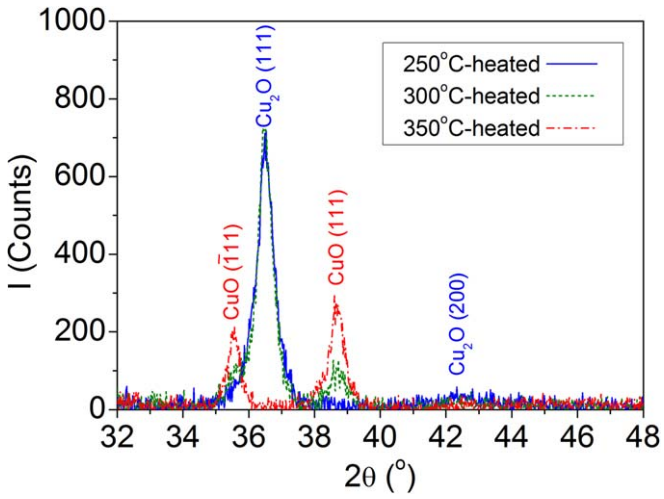

Figure 1. XRD patterns corresponding to copper thin films oxidized at different temperatures.

3. Results and discussion

3.1. Cu_2O thin films obtained by oxidation of evaporated Cu layers

The crystalline structure of copper oxide films is found dependent on the heating temperature, as illustrated by the XRD patterns in figure 1. Cubic Cu_2O with main (111) diffraction (JCPDS no. 05-0667) appears in the form of small crystallites (14 nm diameter) after heating the samples at 250 °C, below the temperature expected from the equilibrium diagram [18]. The increment of the heating temperature to 350 °C produces transition to monoclinic CuO (JCPDS no. 89-5899) with a higher crystallite size (16 nm diameter), while a mixture of Cu_2O and CuO phases is obtained at 300 °C. The formation of Cu_2O at low temperatures is attributed to the surface energy of small particles, which promotes the coalescence of nanocrystallites with high symmetry (cubic). Transition to larger CuO crystallites with a lower symmetry (monoclinic) occurs at superior temperatures, involving a sharp decrease in the normalized cell volume [19].

The electrical conductivity decreases from 1.7×10^{-2} S cm^{-1} for the pure Cu_2O sample to 2.0×10^{-4} S cm^{-1} for the CuO film, being p-type in both compounds and dominated by the carrier concentration, which decreases from 10^{16} cm^{-3} to 10^{14} cm^{-3} ranges. First-principles calculations have stated that copper oxides are p-type semiconductors due to Cu vacancies (V_{Cu}), because they are energetically favored and induce shallow acceptor states at the top of the valence band [20, 21]. Otherwise, copper interstitials (Cu_i) and oxygen vacancies (V_O) create donor levels within the band gap, acting as hole-killer defects [10, 21]. The activation energy for such recombination levels is found lower in CuO than Cu_2O [19], which explains the decrease in free hole densities when CuO crystallizes with increasing temperature. Both Cu_2O and CuO samples show transparency above 85% in the near infrared region (figure 2). In the visible range, the optical absorption is lower for Cu_2O (with $E_g = 2.55$ eV) than for CuO ($E_g = 2.20$ eV), according to other works [22, 23]. Thus, high visible transmittance and acceptable electrical conductance are concurrently achieved with single-phase Cu_2O layers prepared at 250 °C.

3.2. NiO thin films obtained by reactive sputtering from metallic target

Nickel oxide samples prepared by reactive sputtering at 24% O_{pp} show XRD peaks corresponding to the cubic rock-salt structure of NiO (JCPDS No. 4-835), as it is represented in figure 3. Mean crystallite sizes of 33 nm are obtained for these films grown at room temperature, with a lattice constant $a = 0.421$ nm that is higher than expected from the standard powder file (0.418 nm) [24]. Such enlargement in the lattice can be attributed to the presence of nickel vacancies (V_{Ni}) and concomitant formation of Ni^{3+} species. This is because the coexistence of Ni^{2+} and Ni^{3+} produces a local spinel arrangement dispersed in the NiO matrix, which alters the cubic rock-salt structure and increases the lattice parameter [25, 26]. After heating in air at 300 °C or above, the crystallite size enlarges to 42 nm and the lattice constant approaches the standard powder value (figure 3). This indicates annihilation of V_{Ni} defects by the annealing.

The as-grown NiO film exhibits a high p-type conductivity of 0.78 S cm^{-1}, with a carrier concentration of 6.2×10^{18} cm^{-3}. The conductivity decreases by several orders of magnitude after heating, to 4.0×10^{-4} S cm^{-1} at 300 °C and 1.5×10^{-4} S cm^{-1} at 500 °C, owing to the decrease in the free holes concentration to the 10^{14}–10^{13} cm^{-3} range. Figure 4 shows the corresponding optical data, which indicate that

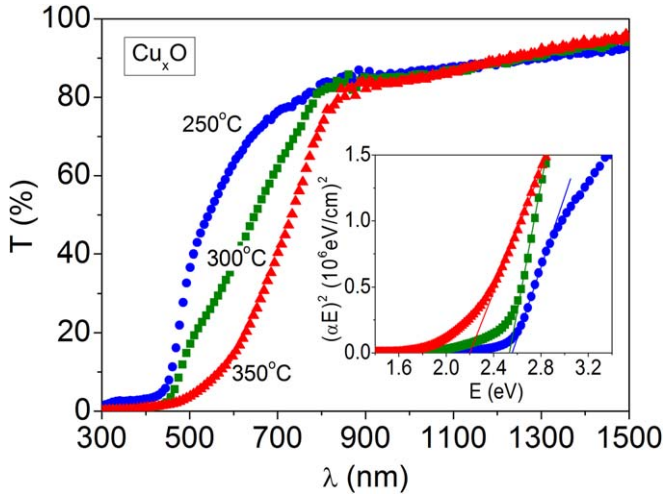

Figure 2. Optical transmittance spectra for the copper oxide thin films at different heating temperatures. The inset shows the respective band-gap energy calculation.

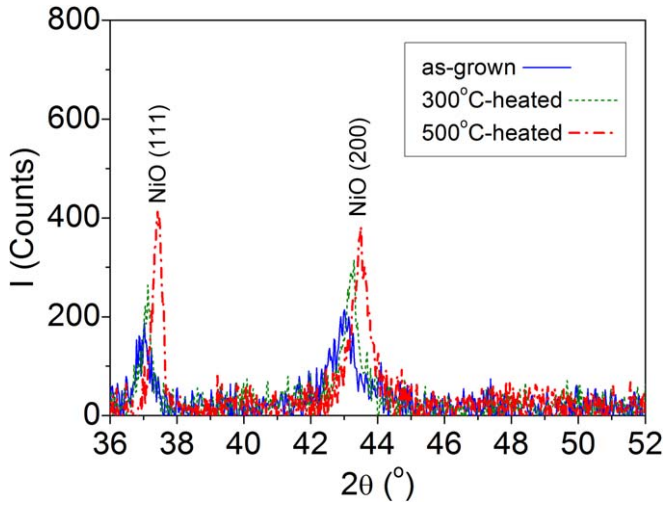

Figure 3. XRD patterns for nickel oxide films grown on unheated substrates and subsequently annealed at various temperatures.

the overall transmittance increases as the electrical conductivity decreases. Such relationship is in accordance with the literature data [27–29], where high conductivity and darkening are attributed to the presence of V_{Ni} defects and subsequent transition of adjacent Ni^{2+} lattice ions into Ni^{3+}, which refers to a structure that contains Ni^{+2} with additional holes localized on Ni sites [29]. The increment in the holes concentration goes along with an increase in the Coulomb attraction between Ni^{3+} and O^{2-}, decreasing the threshold energy of the p–d charge transfer involved in the interbands transition [30]. This results in a transparency decrease by gap narrowing. The band-gap energy, calculated in the inset of figure 4, is found increasing from $E_g = 2.91$ eV for the NiO film as-grown at room temperature to $E_g = 3.66$–3.71 eV after heating at 300 °C–500 °C. In a similar way, the values reported for other nickel oxide films change in the range $E_g = 3.0$–4.0 eV depending on the deposition conditions [27–29]. Despite their higher visible transparency, the heated layers have a very low electrical conductivity due to the annihilation of nickel vacancies by lattice rearrangement when the temperature increased. Therefore, NiO films as-grown at room temperature are more suitable for acting as p-type conductive electrodes.

3.3. SnO thin films obtained by reactive sputtering from Sn target

The tin oxide layers prepared by reactive sputtering at room temperature are found amorphous for the x-ray diffraction [31]. Nevertheless, they show crystallization in the tetragonal SnO structure (JCPDS card No 06-0395) after heating at $T \geqslant 200$ °C, as it is illustrated in figure 5for thin films prepared at 12% O_{pp}. The SnO crystallite size increased from 24 to 30 nm when the temperature was raised from 200 to 450 °C, although some

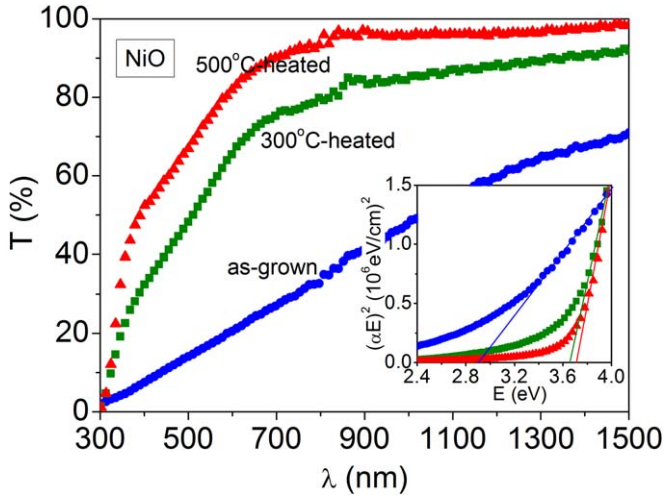

Figure 4. Optical transmittance for the NiO films grown on unheated substrates and subsequently annealed at various temperatures. Gap energy calculation is in the inset.

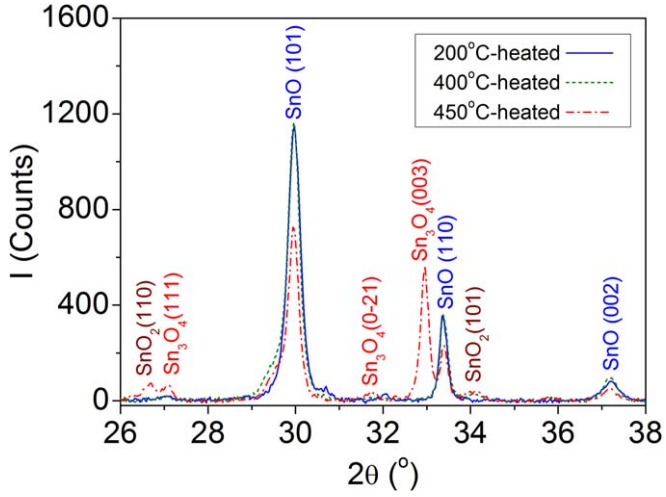

Figure 5. XRD patterns corresponding to tin oxide films heated in air at various temperatures.

additional peaks appeared after heating at the highest temperature. These correspond to tetragonal SnO_2 (JCPDS card No 41-1445) and Sn_3O_4 (JCPDS card No 20-1293), with crystallite sizes of 20 and 35 nm respectively. It should be noted that Sn_3O_4 is an intermediate oxide (with tin in both Sn^{2+} and Sn^{4+} states), which is typically formed during the oxidation from SnO to the most stable SnO_2 phase [32–34].

For these SnO samples, a significant improvement in the optical and electrical properties is obtained by increasing the annealing temperature from 200 to 400 °C. The evolution of the optical transmittance is represented in figure 6, where the highest transparency is observed after heating at 350 °C–400 °C. This corresponds to p-type conductivities of 0.8 S cm^{-1} with free hole densities around 1.5×10^{18} cm^{-3}, attributed to the presence of acceptor defects such as Sn vacancies (V_{Sn}). The band-gap energy calculated in the figure 6 inset achieves a maximum $E_g = 2.93$ eV for the layers heated at 350ºC–400 °C, with no appreciable differences in that temperature range. The subsequent optical and electrical worsening at 450 °C is related to the crystallization of SnO_2 and intermediate oxides in competition with the main SnO, as evidenced by the respective XRD pattern in figure 5. It is known that SnO_2 is intrinsically n-type due to a low formation energy for donor oxygen vacancies [35, 36]. The best optical and electrical performance is then achieved for single-phase SnO layers after annealing at a moderate temperature of about 350 °C.

3.4. Cu_x(S, O) thin films obtained by sulfoxidation of evaporated Cu

The combination of oxygen and sulfur anions has been investigated by the formation of Cu_x(S, O) layers by three different ways: (a) oxidation of CuS, (b) sulfurization of Cu_2O and (c) direct sulfoxidation of metallic copper.

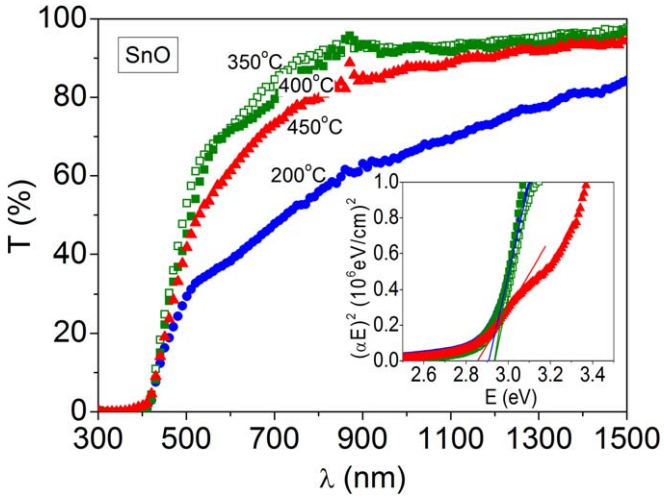

Figure 6. Optical transmittance for the tin oxide films heated in air at various temperatures. The inset shows band-gap energy calculation.

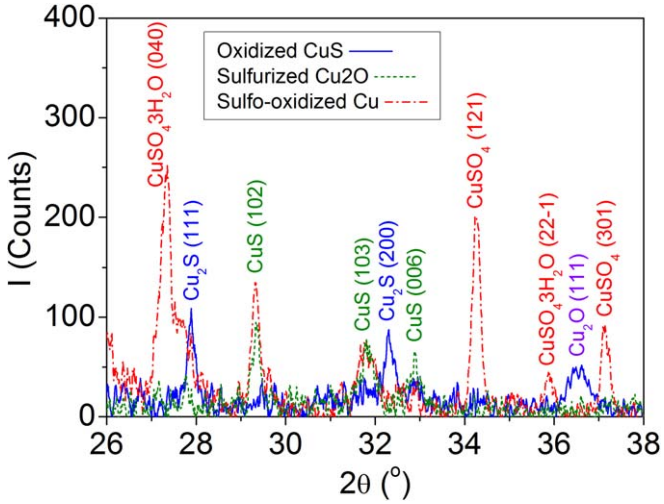

Figure 7. XRD patterns for the $Cu_x(S, O)$ films obtained in different ways.

The various processes were performed at a same temperature of 250 °C, changing the heating atmosphere in one or two steps. The crystalline structure of these samples is analyzed in figure 7. The XRD graph for oxidized CuS shows diffraction peaks corresponding to cubic Cu_2S (JCPDS no. 84-1770) and cubic Cu_2O (JCPDS no. 05-0667), instead of the hexagonal CuS phase (JCPDS no. 06–0464) that was the only one present before the oxidation treatment [37]. The initial CuS layer consisted of crystallites with 34 nm sizes, which have evolved into slightly larger Cu_2S crystallites (36 nm in diameter) along with small Cu_2O crystallites (15 nm average size) during the oxidation process. Analogous evolution from hexagonal CuS to cubic Cu_2S nanocrystals, when heated at 250 °C in flowing nitrogen, has been attributed to a loss of sulfur atoms and subsequent lattice rearrangement [38]. In other way, the Cu_2O sample represented in figure 1 (showing cubic crystallites of 14 nm) has changed to hexagonal CuS with larger crystallites (34 nm in size) after sulfurization. For the direct sulfoxidized copper film, additional peaks have been observed and identified in figure 7. They correspond to orthorhombic $CuSO_4$ (JCPDS no. 15-0775) and monoclinic $CuSO_4{\cdot}3H_2O$ (JCPDS no. 22-0249), with average crystallite sizes of 48 nm and 40 nm, respectively. The coexistence of anhydrous and hydrated $CuSO_4$ phases is commonly found [39, 40]. This is due to the spontaneous formation of hydrated species at ambient pressure and temperature, the reaction of anhydrous to trihydrate being specially favored [40]. The close connections between anhydrous and hydrated phases make possible the aggregation of molecules in crystals with different polymorphisms [41].

The optical data obtained for the different $Cu_x(S, O)$ layers are shown in figure 8. Direct sulfoxidized Cu and oxidized CuS display similar transmittance in the visible range, but a lower transmittance is obtained for the

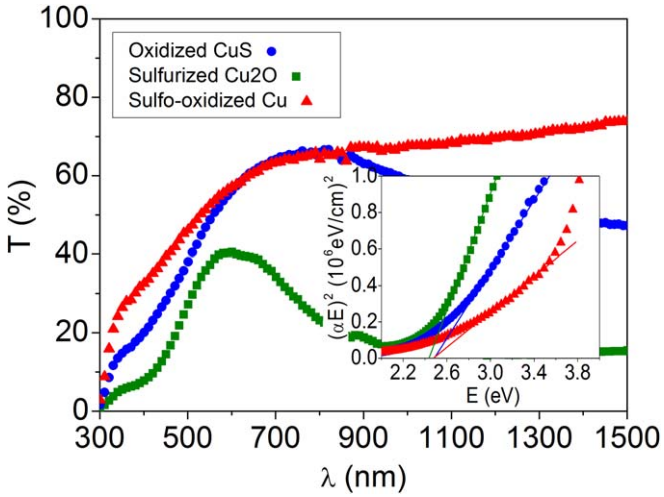

Figure 8. Transmittance spectra for the $Cu_x(S, O)$ films obtained in different ways. The inset shows band-gap energy calculation.

oxidized CuS in the infrared region. A further transmittance decrease (in both visible and infrared wavelengths) is observed for the sulfurized Cu_2O. Nevertheless, the band-gap energy moves in a small range $E_g = 2.44$–2.48 eV for the various samples, as it is calculated in the inset of figure 8. Then, the transmittance variations should be related to the respective holes concentration and subsequent free carrier absorption [42]. For these layers, the transmittance decreases as the carrier concentration increases in the 10^{18}–10^{22} cm^{-3} interval, which is well above the carrier concentration obtained for pure Cu_2O (10^{16} cm^{-3} in the section 3.1). The incorporation of sulfur anions is proven effective to increase the carrier concentration and conductivity, as expected from previous investigations [43]. More specifically, the $Cu_x(S, O)$ films obtained by sulfurization of Cu_2O have achieve the best electrical performance in this work, with a holes density of 1.1×10^{22} cm^{-3} corresponding to p-type conductivity of 2.2×10^2 S cm^{-1}.

3.5. Comparison of the obtained thin film materials as p-type TCOs

In order to evaluate and compare the quality of different layers as transparent and conductive electrodes, a figure of merit is defined by Haacke as [44]: $\Phi_H = T_V^n / R_S = \sigma t e^{-n\alpha_V t}$, which considers the optical characteristics at 550 nm wavelength (transmittance T_V or absorption coefficient α_V) as well as the electrical properties (sheet resistance R_s or conductivity σ). Besides, n is a number that can take different values setting the film thickness and transmittance limits that maximize the function: $t_{max} = 1/(n\alpha_V)$, for which $T_V = e^{-1/n}$. Thus, values of n equal to 2, 4, 8 or 10 place the maximum at visible transmittances of 61%, 78%, 88% or 90%, respectively. Recent studies have pointed out that the resolution of Φ_H decreases when the transmittance power n increases [45], owing to the high predominance of optical characteristics that vary in a relatively small range ($0 \leqslant T_V \leqslant 1$). However, the resolution greatly improves when the power is charged in another way: $\Phi_{H-HR} = T_V / \sqrt[m]{R_S} = (\sigma t)^{1/m} e^{-\alpha_V t}$, giving a new figure of merit named H-HR (Haacke high resolution) [45]. It should be noted that a same film thickness maximizes both Φ_H and $\Phi_{H\text{-}HR}$ functions, since for the last expression it is also $t_{max} = 1/(m\alpha_V)$. The selection of the n or m value depends on the transparent conductor application. In most cases, a visible transmittance of about 80% is considered appropriate, and therefore a value $m = 4$ has been selected to compare the present samples.

Table 1 summarizes the main optical and electrical characteristics for the different metal oxides analyzed in the previous sections. For each material, the respective α_V and σ data have been used to calculate the evolution of the high-resolution figure of merit in function of the film thickness, as it is illustrated in figure 9. This figure shows experimental points corresponding to samples with different thicknesses and also extrapolation lines in a wider range. The highest quality is achieved by the $Cu_2(S, O)$ layers crystallized at 250 °C, which give a maximum $\Phi_{H\text{-}HR} = 0.126\ \Omega^{-1/4}$ at $t \sim 30$ nm, being $\Phi_{H\text{-}HR} \geqslant 0.044\ \Omega^{-1/4}$ for $t \leqslant 230$ nm. For superior thicknesses, the SnO films crystallized at 350 °C achieve a better quality. Moreover, the NiO layers obtained at room temperature have a good quality to be applied on heat-sensitive substrates, with $\Phi_{H\text{-}HR} \geqslant 0.020\ \Omega^{-1/4}$ for $t \leqslant 70$ nm.

4. Conclusions

Several metal oxides (Cu_2O, NiO and SnO) have been prepared, characterized and evaluated as transparent and p-type conductive films, according to the Haacke-high-resolution figure of merit.

Table 1. Summary of the main characteristics obtained for the various compounds. They are included the band-gap energy, absorption coefficient at 550 nm wavelength, p-type conductivity, carrier concentration, mobility and maximum figure of merit achieved for each material.

Compound	Crystallization temperature	E_g (eV)	α_V (cm^{-1})	σ (S cm^{-1})	N (cm^{-3})	μ (cm^2 $V^{-1}s^{-1}$)	$\Phi_{H\text{-}HR}$ ($\Omega^{-1/4}$)
Cu_2O	250 °C	2.55	$5.1x10^4$	$1.7x10^{-2}$	$2.1x10^{16}$	4.6	0.013
NiO	25 °C	2.91	$1.4x10^5$	$7.8x10^{-1}$	$6.2x10^{18}$	0.8	0.027
SnO	350 °C	2.93	$2.0x10^4$	$8.0x10^{-1}$	$1.5x10^{18}$	3.5	0.044
Cu_x(S, O)	250 °C	2.44	$8.0x10^4$	$2.2x10^2$	$1.1x10^{22}$	0.4	0.126

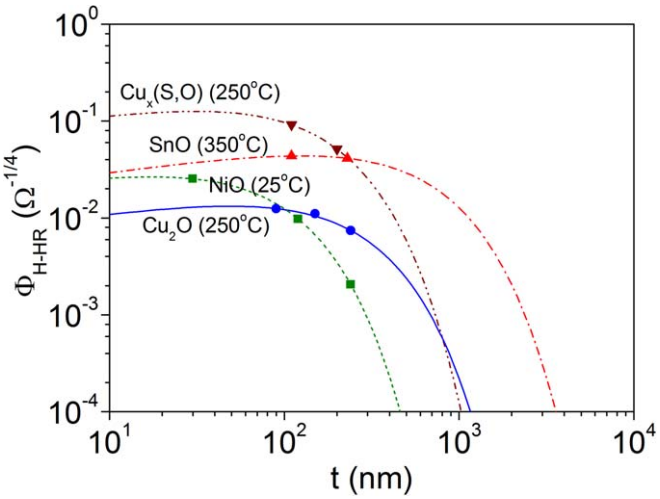

Figure 9. Evolution of the figure of merit ($\Phi_{H\text{-}HR}$) as a function of the thickness for the various thin films developed in the present work. The crystallization temperature for each material is included.

NiO is the only one that exhibits a crystalline structure as-grown at room temperature, with cubic crystallites of 33 nm in size, and some lattice distortion related to the presence of nickel vacancies. These acceptor defects allow achieving a hole density of $6.2x10^{18}$ cm^{-3} and p-type conductivity of 0.78 S cm^{-1}. The optical absorption coefficient is relatively high ($1.4x10^5$ cm^{-1} at 550 nm wavelength) and, therefore, the film thickness should be kept below 70 nm in order to have a figure of merit within the 0.02–0.03 $\Omega^{-1/4}$ range.

The lowest visible absorption (2.0×10^4 cm^{-1} at $\lambda = 550$ nm) corresponds to tetragonal SnO crystallites (26 nm mean size) obtained at 350 °C, with p-type conductivity of 0.80 S cm^{-1}. These SnO layers maintain good quality for a wide range of thicknesses, being the figure of merit in the interval 0.03–0.04 $\Omega^{-1/4}$ for films with t = 10–600 nm.

In comparison, copper oxides show a poor conductivity of 1.7×10^{-2} Scm^{-1} for Cu_2O crystallites (14 nm in size) obtained at 250 °C and lower for CuO crystallized at 350 °C, due to low free carrier concentrations. However, the incorporation of sulfur anions improves the electrical characteristics. In fact, Cu_x(S, O) layers obtained by sulfurization of Cu_2O have reached the highest hole density (1.1×10^{22} cm^{-3}) and p-type conductivity of 2.2×10^2 S cm^{-1}. This corresponds to a figure of merit above 0.10 $\Omega^{-1/4}$ for Cu_x(S, O) film thickness below 100 nm, with a maximum of 0.126 $\Omega^{-1/4}$ for t $\sim$ 30 nm.

Acknowledgments

This work was supported by the Spanish Ministry of Science, Innovation and Universities [grant number MAT2015-66649-R] without any influence on its outcome.

Declarations of interest

None.

ORCID iDs

C Guillén https://orcid.org/0000-0002-7928-8240

References

[1] King P D C and Veal T D 2011 Conductivity in transparent oxide semiconductors *J. Phys. Condens. Matter* **23** 334214
[2] Afre R A, Sharma N, Sharon M M and Sharon M M 2018 Transparent conducting oxide films for various applications: a review *Rev. Adv. Mater. Sci.* **53** 79–89
[3] Casini M 2018 Active dynamic windows for buildings: a review *Renew. Energy.* **119** 923–34
[4] Jang J, Kang Y, Cha D, Bae J and Lee S 2019 Thin-film optical devices based on transparent conducting oxides: Physical mechanisms and applications *Crystals.* **9** 192
[5] Woods-Robinson R, Broberg D, Faghaninia A, Jain A, Dwaraknath S S and Persson K A 2018 Assessing high-throughput descriptors for prediction of transparent conductors *Chem. Mater.* **30** 8375–89
[6] Zhang K H L, Xi K, Blamire M G and Egdell R G 2016 P-type transparent conducting oxides *J. Phys. Condens. Matter* **28** 383002
[7] Wang Z, Nayak P K, Caraveo-Frescas J A and Alshareef H N 2016 Recent developments in p-type oxide semiconductor materials and devices *Adv. Mater.* **28** 3831–92
[8] Hautier G, Miglio A, Ceder G, Rignanese G-M and Gonze X 2013 Identification and design principles of low hole effective mass p-type transparent conducting oxides *Nat. Commun.* **4** 2292
[9] Cao R, Deng H X and Luo J W 2019 Design principles of p-type transparent conductive materials *ACS Appl. Mater. Interfaces* **11** 24837–49
[10] Raebiger H, Lany S and Zunger A 2007 Origins of the p-type nature and cation deficiency in Cu_2O and related materials *Phys. Rev. B* **76** 45209
[11] Osorio-Guillén J, Lany S and Zunger A 2010 Nonstoichiometry and hole doping in NiO *AIP Conf. Proc.* **1199** 128–9
[12] Hosono H 2013 Exploring electro-active functionality of transparent oxide materials *Jpn. J. Appl. Phys.* **52** 90001
[13] Yang T, Zhao J, Li X, Gao X, Xue C, Wu Y and Tai R 2015 Preparation and characterization of p-type transparent conducting SnO thin films *Mater. Lett.* **139** 39–41
[14] Zhang N, Sun J and Gong H 2019 Transparent p-type semiconductors: copper-based oxides and oxychalcogenides *Coatings.* **9** 137
[15] Tang C-J, Ye J-M, Yang Y-T and He J-L 2016 Large-area flexible monolithic ITO/WO_3/Nb_2O_5/NiV$O\chi$/ITO electrochromic devices prepared by using magnetron sputter deposition *Opt. Mater. (Amst).* **55** 83–9
[16] Guillén C and Herrero J 2003 Low-resistivity Mo thin films prepared by evaporation onto 30 cm × 30 cm glass substrates *J. Mater. Process. Technol.* **143–144** 144–7
[17] Guillén C and Herrero J 2005 Influence of the thickness and the oxygen content on the characteristics of ITO thin films deposited at room temperature by in-line sputtering on large areas ed W Palz *et al 20th Eur. Photovolt. Sol. Energy Conf., WIP-Renewable Energies (Barcelona)* pp 1859–62
[18] Heinemann M, Eifert B and Heiliger C 2013 Band structure and phase stability of the copper oxides Cu_2O, CuO, and Cu_4O_3 *Phys. Rev. B* **87** 115111
[19] Guillén C and Herrero J 2018 Single-phase Cu_2O and CuO thin films obtained by low-temperature oxidation processes *J. Alloys Compd.* **737** 718–24
[20] Scanlon D O, Morgan B J, Watson G W and Walsh A 2009 Acceptor levels in p-type Cu_2O: rationalizing theory and experiment *Phys. Rev. Lett.* **103** 96405
[21] Wu D, Zhang Q and Tao M 2006 LSDA + U study of cupric oxide: electronic structure and native point defects *Phys. Rev. B* **73** 235206
[22] Shanid N A M and Khadar M A 2008 Evolution of nanostructure, phase transition and band gap tailoring in oxidized Cu thin films *Thin Solid Films* **516** 6245–52
[23] Figueiredo V, Elangovan E, Gonçalves G, Barquinha P, Pereira L, Franco N, Alves E, Martins R and Fortunato E 2008 Effect of post-annealing on the properties of copper oxide thin films obtained from the oxidation of evaporated metallic copper *Appl. Surf. Sci.* **254** 3949–54
[24] Guillén C and Herrero J 2019 Transparent and p-type conductive Ni_xO:V thin films obtained by reactive DC sputtering at room temperature *Mater. Res. Express* **6** 96410
[25] Vidales-Hurtado M A and Mendoza-Galván A 2008 Optical and structural characterization of nickel oxide-based thin films obtained by chemical bath deposition *Mater. Chem. Phys.* **107** 33–8
[26] Mendoza-Galván A, Vidales-Hurtado M A and López-Beltrán A M 2009 Comparison of the optical and structural properties of nickel oxide-based thin films obtained by chemical bath and sputtering *Thin Solid Films* **517** 3115–20
[27] Nandy S, Saha B, Mitra M K and Chattopadhyay K K 2007 Effect of oxygen partial pressure on the electrical and optical properties of highly (200) oriented p-type $Ni_{1-x}O$ films by DC sputtering *J. Mater. Sci.* **42** 5766–72
[28] Chuang T-H, Wen C-K, Peng W-C, Wang X, Sun H and Chen S-C 2018 The influence of oxygen flow ratio on the optoelectronic properties of p-type $Ni_{1-x}O$ films deposited by ion beam assisted sputtering *Coatings.* **8** 168
[29] Hwang J D and Ho T H 2017 Effects of oxygen content on the structural, optical, and electrical properties of NiO films fabricated by radio-frequency magnetron sputtering *Mater. Sci. Semicond. Process.* **71** 396–400
[30] Ono M, Sasaki K, Nagai H, Yamaguchi T, Higashiwaki M, Kuramata A, Yamakoshi S, Sato M, Honda T and Onuma T 2018 Relation between electrical and optical properties of p-type NiO films *Phys. Status Solidi Basic Res.* **255** 1–5
[31] Guillén C and Herrero J 2019 P-type SnO thin films prepared by reactive sputtering at high deposition rates *J. Mater. Sci. Technol.* **35** 1706–11
[32] Batzill M and Diebold U 2005 The surface and materials science of tin oxide *Prog. Surf. Sci.* **79** 47–154
[33] Seko A, Togo A, Oba F and Tanaka I 2008 Structure and stability of a homologous series of tin oxides *Phys. Rev. Lett.* **100** 45702
[34] Zhang F, Lian Y, Gu M, Yu J and Tang T B 2017 Static and dynamic disorder in metastable phases of tin oxide *J. Phys. Chem. C* **121** 16006–11
[35] Kílíç C and Zunger A 2002 Origins of coexistence of conductivity and transparency in SnO_2 *Phys. Rev. Lett.* **88** 95501
[36] Guillén C and Herrero J 2019 Intrinsic and extrinsic doping contributions in SnO_2 and SnO_2:Sb thin films prepared by reactive sputtering *J. Alloys Compd.* **791** 68–74
[37] Guillén C and Herrero J 2018 Copper oxy-sulfide and copper sulfate thin films as transparent p-type conductive electrodes *Mater. Res. Bull.* **101** 116–22

[38] Liu L, Liu C, Fu W, Deng L and Zhong H 2016 Phase transformations of copper sulfide nanocrystals: towards highly efficient quantum-dot-sensitized solar cells *ChemPhysChem* **17** 771–6
[39] Xia J, Yu D, Hu Y, Zou B, Sun P, Li H and Huang H 2011 Sulfated copper oxide: an efficient catalyst for dehydration of sorbitol to isosorbide *Catal. Commun.* **12** 544–7
[40] Ruggiero M T, Bardon T, Strlič M, Taday P F and Korter T M 2014 Assignment of the terahertz spectra of crystalline copper sulfate and its hydrates via solid-state density functional theory *J. Phys. Chem. A.* **118** 10101–8
[41] Singh M, Kumar D, Thomas J and Ramanan A 2010 Crystallization of copper(II) sulfate based minerals and MOF from solution: chemical insights into the supramolecular interactions *J. Chem. Sci.* **122** 757–69
[42] Wang L, Ren B, Weng L, Huang J, Tang K and Yang Y 2015 Metal-semiconductor transition in CuS-$Cu_{1.8}S$ mixed phase thin films *Vacuum* **112** 70–2
[43] Guillén C and Herrero J 2017 Nanocrystalline copper sulfide and copper selenide thin films with p-type metallic behavior *J. Mater. Sci.* **52** 13886–96
[44] Haacke G 1976 New figure of merit for transparent conductors *J. Appl. Phys.* **47** 4086–9
[45] Cisneros-Contreras I R, Muñoz-Rosas A L and Rodríguez-Gómez A 2019 Resolution improvement in Haacke's figure of merit for transparent conductive films *Results Phys.* **15** 102695